Efficient Monolithic Perovskite/Perovskite Tandem Solar Cells

Dávid Forgács, Lidón Gil-Escrig, Daniel Pérez-Del-Rey, Cristina Momblona, Jérémie Werner, Bjoern Niesen, Christophe Ballif, Michele Sessolo, and Henk J. Bolink*

Organic–inorganic (hybrid) perovskites are at the forefront of emerging photovoltaic materials, thanks to their fast rising and constantly improving power conversion efficiencies (PCEs), which are now exceeding 22%.[1–6] While the development of novel absorber materials is likely to further enhance the performances of perovskite solar cells, the use of novel architectures such as tandem cells is a proven successful strategy to overcome the Shockley–Queisser limit of single junction devices. Hybrid perovskites are quite unique, being efficient semiconductors whose bandgap can be readily tuned over a wide range, allowing light absorption from near-infrared to visible wavelengths.[7,8] For this reason, they are being investigated as top cells in combination with a variety of narrow bandgap solar cells,[9–12] in particular with silicon[7,13–17] and copper indium gallium selenide.[15,18–20] The challenges associated with the advance of perovskite tandem solar cells include the development of charge recombination layers (CRLs) between the two subcells with low ohmic losses and of deposition processes that are compatible with the underline photovoltaic cells. Hence, most of the reported tandem devices consist in mechanically stacked semitransparent cells (4-terminal cells), while only few recent examples have demonstrated the fabrication of monolithic, 2-terminal photovoltaic devices.[21–25] An alternative strategy is the development of perovskite–perovskite tandem devices, which could profit from the simple bandgap tuning of perovskite absorbers and from the use of inexpensive precursor materials. The first example of perovskite–perovskite tandem used two analogue subcells with the same absorbing material, methylammonium lead iodide ($MAPbI_3$), which were connected by lamination with a 2 μm thick, doped hole transport layer (HTL).[26] Despite the demonstration of an open-circuit voltage (V_{oc}) as high as 2.2 V (the exact sum of the photovoltage produced by the two subcells), the PCE was limited by the use of the same absorber, which in turn strongly reduced the overall attainable current density. In another work, a monolithic perovskite–perovskite tandem device was fully solution processed using a multilayer organic CRL, which is challenging due to the requirement of solvent orthogonality during processing of each of the layers.[27] Also in this case the two subcells used an identical perovskite absorber, $MAPbI_3$, hence limiting the overall PCE. In order to prepare efficient tandem structures, the development of complementary, narrow bandgap perovskite materials is also being pursued.[28] Recently, Yang et al. presented the narrow bandgap (1.33 eV) $MA_{0.5}FA_{0.5}Pb_{0.75}Sn_{0.25}I_3$ perovskite, which could lead to single junction cells with a PCE of 14.19%.[29] They also fabricated a 4-terminal tandem using the narrow bandgap mixed perovskite in combination with a semitransparent $MAPbI_3$ cell (used as the wide bandgap material), achieving a PCE of about 19%. In general, the deposition of the CRL remains challenging, since it has to fulfill the requirements of high transparency, high conductivity, and at the same time the deposition process must be compatible with the underlying perovskite and organic transport layers. A valuable alternative in the preparation of tandem solar cells is the use of doped organic semiconductors, which have been widely studied for tandem organic light-emitting diodes and small molecular weight organic photovoltaics.[30–32] In these materials the conductivity can be tuned over several orders of magnitude by simply varying the dopant concentration, yet maintaining a high optical transmittance.[33] Importantly, organic semiconductors can be processed by simple vacuum deposition techniques which are intrinsically additive, meaning that multilayer devices can be built without chemical modifications of the underlying layers or the use of orthogonal solvents.[34,35] The low fabrication temperature makes vacuum deposition compatible with any underlying active material and in general with a wide range of substrates, including flexible and textiles. Also, vacuum deposited films are able to conform with the substrate morphology, an important feature in the preparation of tandem devices on textured silicon cells.[24]

In this work we present efficient monolithic tandem solar cells based on two perovskite absorbers with different and complementary bandgaps. For the front subcell, a wide bandgap perovskite with composition $Cs_{0.15}FA_{0.85}Pb(I_{0.3}Br_{0.7})_3$ was used as the absorber.[28] The rear subcell used the well-known narrow bandgap perovskite $MAPbI_3$ as the absorber. The wide bandgap perovskite is solution processed yet the remaining materials needed to construct the tandem devices are all deposited using thermal evaporation. By employing doped organic semiconductors, an efficient extraction and transport of the photogenerated

D. Forgács, L. Gil-Escrig, D. Pérez-Del-Rey, C. Momblona, Dr. M. Sessolo, Dr. H. J. Bolink
Instituto de Ciencia Molecular
Universidad de Valencia
C/J. Beltrán 2, 46980 Paterna, Spain
E-mail: michele.sessolo@uv.es
J. Werner, Dr. B. Niesen, Prof. C. Ballif
Ecole Polytechnique Fédérale de Lausanne (EPFL)
Institute of Microengineering (IMT)
Photovoltaics and Thin-Film Electronics Laboratory
Rue de la Maladière 71b, 2002 Neuchâtel, Switzerland
Dr. B. Niesen, Prof. C. Ballif
CSEM
PV-Center
Rue Jaquet-Droz 1, 2002 Neuchâtel, Switzerland

charge carriers is ensured, while carrier recombination at the perovskite interfaces is prohibited by using intrinsic and selective charge transport layers. Despite the nonideal combination of bandgaps in the two subcells, we demonstrate perovskite–perovskite tandem cells delivering an average PCE of 15%, and a record efficiency of 18%. This work demonstrates the potential of vacuum deposited multilayer structures in overcoming the efficiency of state of the art perovskite solar cells.

Thin films of the mixed perovskite $Cs_{0.15}FA_{0.85}Pb(I_{0.3}Br_{0.7})_3$ have been prepared from solution following a recently published protocol (details in the Supporting Information).[28] This particular composition has been reported to lead to a semiconducting perovskite with an optical bandgap of ≈2 eV, which would maximize the efficiency of a tandem device when the absorber of the second subcell is $MAPbI_3$, with a bandgap of 1.55 eV.[36]

$MAPbI_3$ layers have been prepared by dual source vapor deposition in a high vacuum chamber using a published procedure (details of the deposition can be found in the Supporting Information).[37] The optical absorption spectra and grazing incidence X-ray diffraction (GIXRD) patterns of both perovskite thin films are depicted in **Figure 1**a,b, respectively, and essentially confirm the formation of highly absorbing polycrystalline perovskite thin films.[28,37] Small molecular weight, sublimable organic semiconductors were employed to form selective charge transporting layers adjacent to the perovskite absorbers in the tandem structure. The optimization of these materials and their dopants, in combination with the $MAPbI_3$ perovskite absorber for single junction solar cells, was recently described by Momblona et al.[38] In Figure 1c, the chemical structures of the charge transport molecules and of their dopants used in this work are reported. As the hole transport material, we have used the N4,N4,N4″,N4″-tetra([1,1′-biphenyl]-4-yl)-[1,1′:4′,1″-terphenyl]-4,4″-diamine (TaTm), whose conductivity can be tuned by two orders of magnitude by doping it with 2,2′-(perfluoronaphthalene-2,6-diylidene) dimalononitrile (F_6-TCNNQ).[38] The fullerene C_{60} was selected as the electron transport material as it has been used as an efficient electron acceptor in perovskite solar cells.[39] Efficient modulation of the C_{60} conductivity can be obtained by codeposition with N1,N4-bis(tri-p-tolylphosphoranylidene) benzene-1,4-diamine (PhIm).[38] The fullerene derivative indene-C_{60}-propionic acid hexyl ester (IPH) was used as a solution-processable interlayer on top of TiO_2, in order to reduce surface recombination and enhance photovoltage (Figure S1, Supporting Information).[28,40] Hence, only the TiO_2 electron transport layer (ETL) and the wide bandgap perovskite absorber are solution processed in this monolithic tandem architecture. This method was selected as mixed ion perovskite preparation using simultaneous sublimation of multiple precursor compounds is rather complicated and still under development. Prior to the integration into monolithic tandem devices, the subcell absorbers were evaluated in single-junction solar cells. The single junction $MAPbI_3$ cells were fully vacuum deposited onto ITO-coated glass slides, using an n–i–p architecture (ETL is deposited on the transparent conductor), as shown in **Figure 2**a. Briefly, a 40 nm thick film of C_{60}:PhIm (60 wt%) (C_{60} doped with PhIm at 60% in weight) is deposited onto the ITO, followed by a 10 nm thick intrinsic C_{60} ETL, which selectively transports electrons confining the holes in the active layer. Subsequently, the $MAPbI_3$ perovskite absorber (500 nm) is deposited by dual source vapor deposition without any thermal treatment. Then, a thin intrinsic TaTm hole transport layer (HTL, 10 nm) is deposited on the perovskite followed by a 40 nm thick TaTm:F_6-TCNNQ

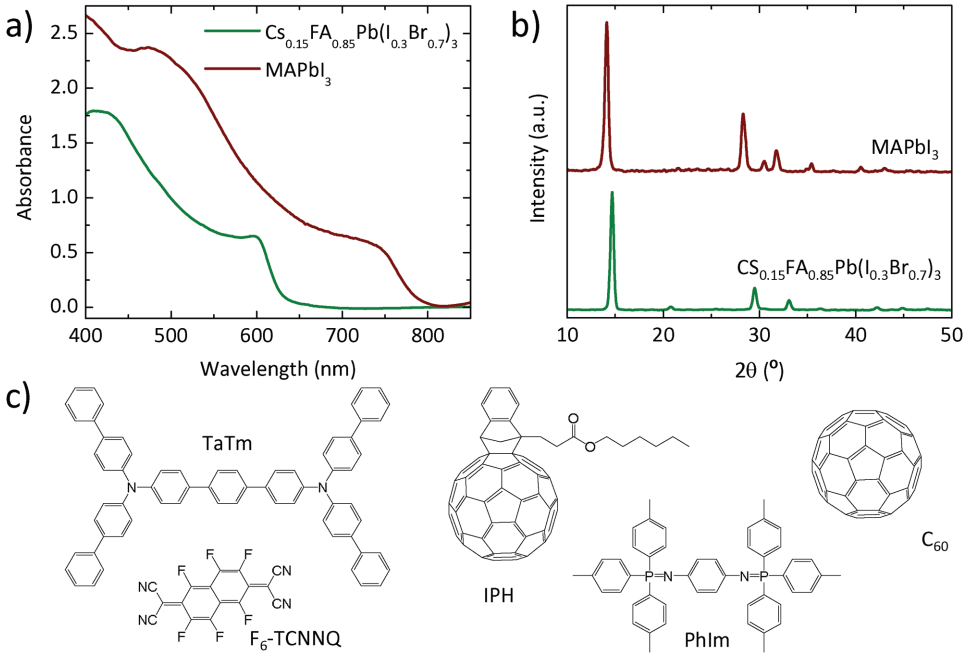

Figure 1. Characterization of perovskite thin films. a) Absorption spectra of $Cs_{0.15}FA_{0.85}Pb(I_{0.3}Br_{0.7})_3$ (300 nm) and $MAPbI_3$ (500 nm). b) GIXRD patterns for the same perovskite films. c) Chemical structures of the organic semiconductors and dopants used as charge transport layers in the photovoltaic devices.

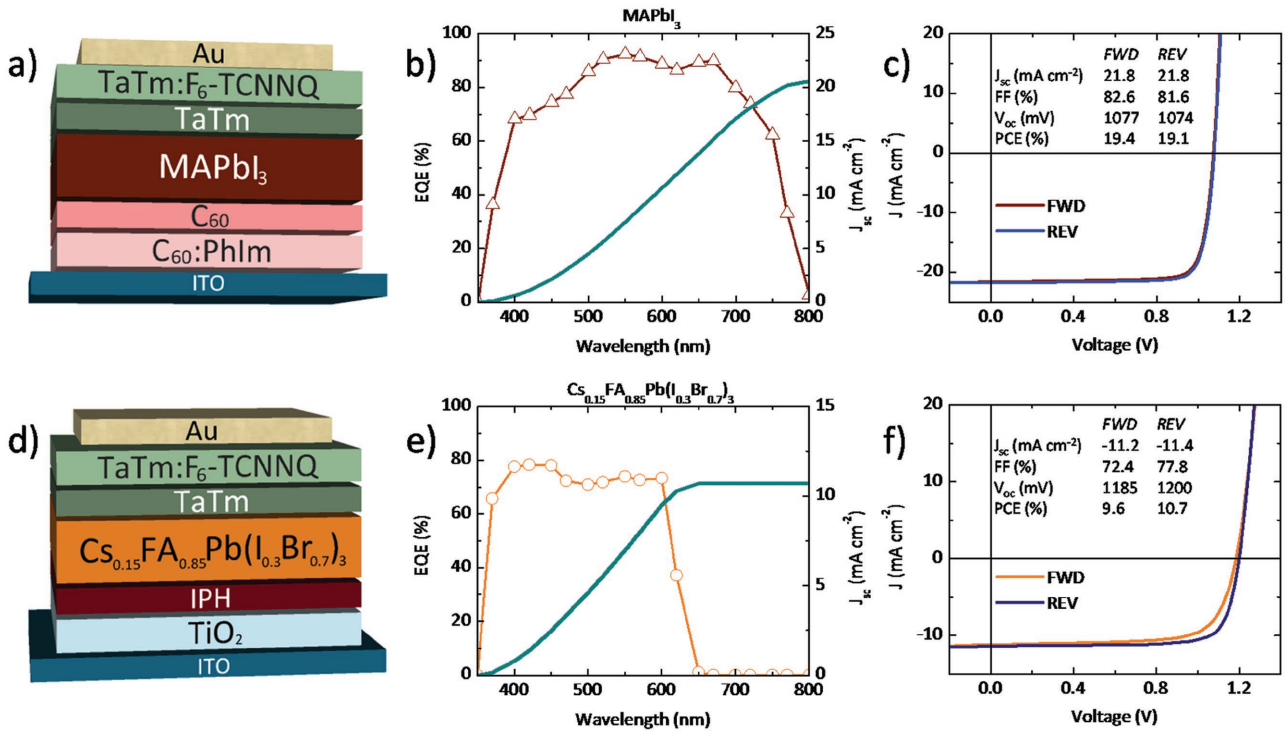

Figure 2. Characterization of single junction perovskite solar cells: a,d) device structures, b,e) external quantum efficiencies (EQE, left), with corresponding integrated photocurrent with the AM1.5G solar spectrum (right axis), and c,f) *J–V* curves under 100 mW cm^{-2} illumination in forward (FWD) and reverse (REV) bias, for a fully vacuum deposited n–i–p $MAPbI_3$ cell and for the wide bandgap perovskite device, respectively.

(11 wt%) film. The device is finished with the deposition of a gold electrode.

Single junction cells based on the wide bandgap absorber $Cs_{0.15}FA_{0.85}Pb(I_{0.3}Br_{0.7})_3$ were built using an n–i–p architecture as well (Figure 2d, details in the Supporting Information). In this case, the ITO was coated with an 80 nm thick TiO_2 ETL prepared by spin-coating of NPs suspensions (diameter 15–20 nm) and annealed at 200 °C for 30 min. Afterward, a thin (10–20 nm) layer of IPH was solution processed from its chlorobenzene solution and annealed at 70 °C for 10 min. The mixed perovskite was spin-coated on top of the IPH from a dimethyl sulfoxide solution, and annealed at 70 °C for 30 s and at 100 °C for 1 h. Besides a partial removal of the IPH during the deposition of the perovskite films, the presence of IPH had a beneficial effect on the device photovoltage (Figure S1, Supporting Information), most likely due to a diminished carrier recombination. Following the perovskite layer formation, a thin (10 nm) intrinsic TaTm HTL and a 40 nm thick TaTm:F_6-TCNNQ (11 wt%) layer were vacuum deposited on the perovskite and capped with a gold electrode.

The devices were first characterized measuring their external quantum efficiency (EQE) as a function of the incident light wavelength (Figure 2b). The optimized $MAPbI_3$ cells, as recently described,[38] show a very high photocurrent response over the whole visible spectrum, with EQE as high as 90% between 500 and 700 nm. This is a consequence of the high absorbance of the perovskite films and of the very low optical absorption characteristic of the doped C60:PhIm film (Figure S2, Supporting Information) used at the front contact. Such high EQE results in a short-circuit current density (J_{sc}) exceeding 20 mA cm^{-2}, in accordance with previous results on analogous devices. The current density versus voltage (*J–V*) characteristics under 100 mW cm^{-2} illumination for the best cell measured during this set of experiments is reported in Figure 2c. The curve shows a very high fill factor (FF, >80%) and V_{oc}, resulting from the efficient extraction of the charge carriers due to the doped interfaces and to a low charge recombination. The solar cell shows negligible *J–V* hysteresis with a PCE exceeding 19%, both when measured in forward (FWD, from J_{sc} to V_{oc}) and in reverse (REV, from V_{oc} to J_{sc}) bias.

The average values of the photovoltaic parameters with their standard deviation (SD), calculated on 16 $MAPbI_3$ cells and measured under forward as well as in reverse bias, are reported in **Table 1**. We obtained an average PCE of 17.3% and 17.4% in forward and reverse bias, respectively, with a SD of less than 2% and the small cell-to-cell variability mainly determined by the photocurrent and FF. The obtained wide bandgap solar cells show a high photocurrent response over the whole visible spectrum, with EQE of 70 to 80% until 600 nm, where the spectral response drops since it coincides with the perovskite bandgap (Figure 2e). The lower spectral EQE (when compared to the $MAPbI_3$ cells) is likely due to the relatively thin absorber used, which is limited by the solubility of the CsBr precursor in dimethyl sulfoxide. The EQE results in a J_{sc} exceeding 10 mA cm^{-2} on average (Table 1). The *J–V* characteristics under 100 mW cm^{-2} illumination for the best cell measured during this set of experiments is reported in Figure 2f. Similar to most metal oxide containing perovskite solar cells, we observed a small but noticeable current hysteresis, with a reduced FF in the forward bias scan. For the record cell, this translates into

Table 1. Performance overview for single-junction perovskite solar cells obtained in forward (FWD) and reverse (REV) bias. The average (Avg.) values with their standard deviation (SD) are reported and compared with their maximum (Max).

	$MAPbI_3$					
	FWD			REV		
	Avg.	SD	Max	Avg.	SD	Max
V_{oc} [mV]	1059	±16	1079	1074	±22	1103
J_{sc} [mA cm^{-2}]	−20.64	±0.75	−21.89	−20.54	±0.79	−21.89
FF [%]	78.8	±3.4	82.6	79.0	±2.5	81.6
PCE [%]	17.3	±1.4	19.4	17.4	±1.1	19.1
	$Cs_{0.15}FA_{0.85}Pb(I_{0.3}Br_{0.7})_3$					
	FWD			REV		
	Avg.	SD	Max	Avg.	SD	Max
V_{oc} [mV]	1159	±32	1194	1167	±42	1215
J_{sc} [mA cm^{-2}]	−10.42	±0.59	−11.22	−10.24	±0.57	−11.41
FF [%]	68.5	±3.3	72.4	75.6	±5.1	81.2
PCE [%]	8.3	±0.9	9.6	9.0	±1.0	10.7

a difference in PCE from 10.7% in reverse bias to 9.6% when the solar cell is forward biased. V_{oc} values as high as 1.2 V have been recorded, the average lying at about 1160 mV, which is in line with those presented previously, but still low taking into account the bandgap of the absorber (≈2 eV).[28] We obtained an average PCE of 8.3% and 9.0% in forward and reverse bias, respectively, with the cell-to-cell variability mainly determined by V_{oc}, and the *J*–*V* hysteresis being correlated with the variation of the FF.

The fabrication of the monolithic perovskite–perovskite tandem starts with the processing of the wide bandgap $Cs_{0.15}FA_{0.85}Pb(I_{0.3}Br_{0.7})_3$ cell as described before, which instead of being finished with the gold electrode, is completed by direct deposition of the full $MAPbI_3$ stack, as represented in **Figure 3**a.

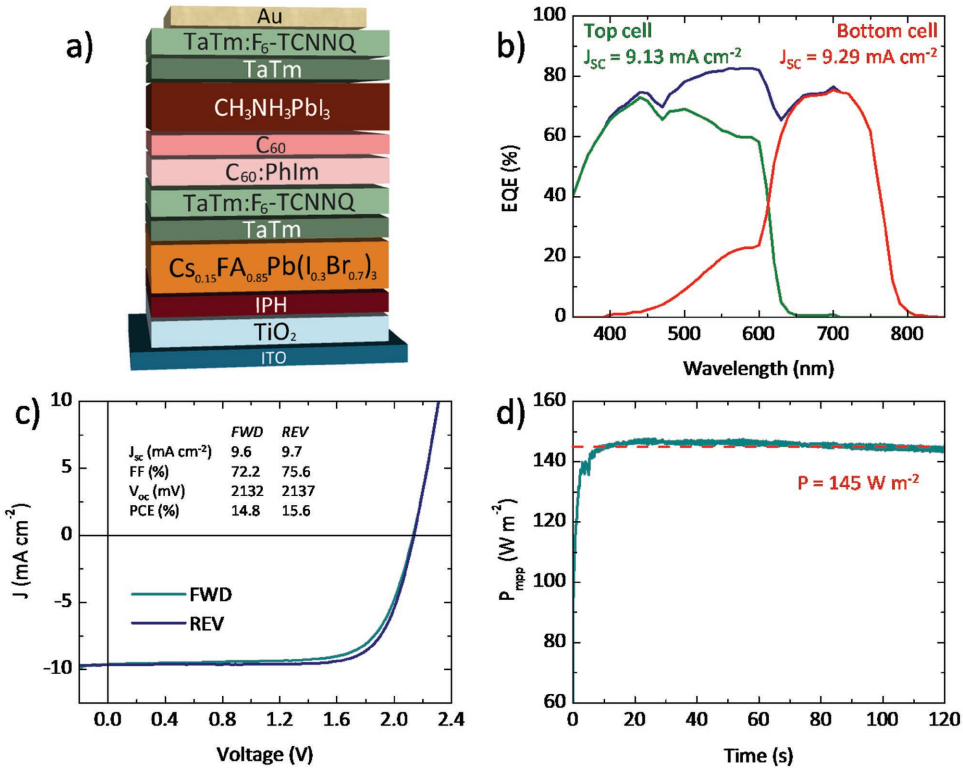

Figure 3. Characterization of monolithic perovskite-perovskite solar cells: a) device structure, b) external quantum efficiency (EQE, left), with highlighted the measured photocurrent density for each subcell. c) *J*–*V* curves under 100 mW cm^{-2} illumination in forward (FWD) and reverse (REV) bias, and d) steady power output under maximum power point tracking for the same device.

In this way the layer stack in between the two different perovskite absorbers consist of a p-doped HTL and an n-doped ETL, TaTm:F_6-TCNNQ (40 nm)/C_{60}:PhIm (40 nm), that is known to function efficiently as a charge recombination layer. Vacuum deposition allows to circumvent the challenges associated with the monolithic integration of two subcells, since no damage of the underlying layer can occur and no thermal treatment is needed. The EQE spectra for a tandem device are reported in Figure 3b, where the contribution for each subcell with corresponding current density is highlighted. The wide bandgap cell delivers a current density of 9.13 mA cm^{-2}, while the bottom $MAPbI_3$ cell produces a slightly higher current of 9.29 mA cm^{-2}, which brings the tandem close to the current-matched situation.

The *J–V* characteristics show only small hysteresis (lower when compared to the single junction wide bandgap cell), with a FF of 72.2% and 75.6% when the cell is measured in forward and reverse bias, respectively (Figure 3c). Importantly, a V_{oc} as high as 2132 and 2137 mV was observed in forward and reverse bias, respectively. From the average photovoltaic parameters (estimated from 48 tandem cells, **Table 2**), one can see how the average V_{oc} obtained from the tandem devices in both reverse and forward bias is very close to the sum of the average photovoltage of each subcell (Table 1), which highlights the high quality of the CRL and in general of the device architecture used. The average PCE for the tandem cell is 14.8% in forward and 15.6% in reverse bias, again due to the slightly higher FF observed when measuring the cells from open to short-circuit. Interestingly, the steady power output measured under maximum power point tracking shows a steady-state efficiency of 14.5% (145 W m^{-2}) after 2 min of illumination, within the average PCE observed (Table 2). The top performing device exhibited a PCE of 18.1% in reverse bias, which is important considering that the theoretical maximum PCE for this bandgap pair lies in the 20%–25% range.[36] In the best performing device, the V_{oc} approaches 2.3 V, which is the exact sum of the record V_{oc} obtained for the 2 subcells. To address the stability of the materials and the device architecture, encapsulated devices were kept in ambient conditions and measured for several days after preparation. The device performance of the cells kept in the dark during several days was, after a short period of illumination, almost identical to that observed on the first day. These preliminary data indicate that these devices have a promising stability (Figure S3, Supporting Information), maintaining more than 98% of the original PCE after 3 d.

Table 2. Performance overview for monolithic perovskite–perovskite solar cells obtained in forward (FWD) and reverse (REV) bias. The average (Avg.) values with their standard deviation (SD) obtained from 48 cells, and the photovoltaic parameters for the best performing device are reported.

	FWD		REV		Record cell	
	Avg.	SD	Avg.	SD	FWD	REV
V_{oc} [mV]	2206	±48	2192	±61	2281	2294
J_{sc} [mA cm^{-2}]	−9.48	±0.44	−9.35	±0.43	−10.01	−9.83
FF [%]	70.7	±4.0	74.3	±5.2	76.1	80.3
PCE [%]	14.8	±1.5	15.3	±1.5	17.4	18.1

The performances of perovskite/perovskite tandem devices presented here are extremely promising and were enabled by the use of doped and intrinsic small-molecule organic semiconductors. Furthermore, these results validate vacuum deposition as a relevant tool in the development of efficient perovskite solar cells, which is important considering that vacuum coating techniques are the standard in the semiconductor industry. Notably, by choosing more appropriate complementary bandgaps, for example, by exchanging the $MAPbI_3$ absorber for a narrower bandgap perovskite, efficiencies in excess of those demonstrated for single junction perovskite solar cells are achievable.

Supporting Information

Supporting Information is available from the --- or from the author.

Acknowledgements

The authors are grateful to Novaled GmbH, in particular to Jan Blochwitz-Nimoth for the supply of the organic charge transport materials and dopandts. The authors further acknowledge financial support from the European Union H2020 project INFORM (Grant No. 675867), the Spanish Ministry of Economy and Competitiveness (MINECO) via the Unidad de Excelencia María de Maeztu MDM-2015-0538, MAT2014-55200-R, and PCIN-2015-255 and the Generalitat Valenciana (Prometeo/2016/135). C.M. and M.S. thank the MINECO for their pre- and post-doctoral (JdC) contracts. The project comprising this work is evaluated by the Swiss National Science Foundation and funded by the Nano-Tera.ch project "Synergy" and by the PNR 70 project "PV2050" with financing from the Swiss National Science Foundation and by the Swiss Federal Office of Energy, under Grant No. SI/501072-01.

[1] W. S. Yang, J. H. Noh, N. J. Jeon, Y. C. Kim, S. Ryu, J. Seo, S. I. Seok, *Science* **2015**, *348*, 1234.
[2] D. Bi, W. Tress, M. I. Dar, P. Gao, J. Luo, C. Renevier, K. Schenk, A. Abate, F. Giordano, J.-P. Correa Baena, J.-D. Decoppet, S. M. Zakeeruddin, M. K. Nazeeruddin, M. Grätzel, A. Hagfeldt, *Sci. Adv.* **2016**, *2*, e1501170.
[3] M. Saliba, T. Matsui, J.-Y. Seo, K. Domanski, J.-P. Correa-Baena, M. K. Nazeeruddin, S. M. Zakeeruddin, W. Tress, A. Abate, A. Hagfeldt, M. Gratzel, *Energy Environ. Sci.* **2016**, *9*, 1989.
[4] T. Jesper Jacobsson, J.-P. Correa-Baena, M. Pazoki, M. Saliba, K. Schenk, M. Gratzel, A. Hagfeldt, *Energy Environ. Sci.* **2016**, *9*, 1706.
[5] X. Li, D. Bi, C. Yi, J.-D. Décoppet, J. Luo, S. M. Zakeeruddin, A. Hagfeldt, M. Grätzel, *Science* **2016**, *353*, 58.
[6] M. A. Green, K. Emery, Y. Hishikawa, W. Warta, E. D. Dunlop, *Prog. Photovolt: Res. Appl.* **2016**, *24*, 905.
[7] C. D. Bailie, M. D. McGehee, *MRS Bull.* **2015**, *40*, 681.
[8] T. Todorov, O. Gunawan, S. Guha, *Mol. Syst. Des. Eng.* **2016**, DOI: 10.1039/C6ME00041J.
[9] T. Todorov, T. Gershon, O. Gunawan, C. Sturdevant, S. Guha, *Appl. Phys. Lett.* **2014**, *105*, 173902.
[10] C.-C. Chen, S.-H. Bae, W.-H. Chang, Z. Hong, G. Li, Q. Chen, H. Zhou, Y. Yang, *Mater. Horiz.* **2015**, *2*, 203.

[11] Y. Liu, L. A. Renna, M. Bag, Z. A. Page, P. Kim, J. Choi, T. Emrick, D. Venkataraman, T. P. Russell, *ACS Appl. Mater. Interfaces* **2016**, *8*, 7070.
[12] J. Liu, S. Lu, L. Zhu, X. Li, W. C. H. Choy, *Nanoscale* **2016**, *8*, 3638.
[13] P. Loper, S.-J. Moon, S. Martin de Nicolas, B. Niesen, M. Ledinsky, S. Nicolay, J. Bailat, J.-H. Yum, S. De Wolf, C. Ballif, *Phys. Chem. Chem. Phys.* **2015**, *17*, 1619.
[14] F. Lang, M. A. Gluba, S. Albrecht, J. Rappich, L. Korte, B. Rech, N. H. Nickel, *J. Phys. Chem. Lett.* **2015**, *6*, 2745.
[15] C. D. Bailie, M. G. Christoforo, J. P. Mailoa, A. R. Bowring, E. L. Unger, W. H. Nguyen, J. Burschka, N. Pellet, J. Z. Lee, M. Gratzel, R. Noufi, T. Buonassisi, A. Salleo, M. D. McGehee, *Energy Environ. Sci.* **2015**, *8*, 956.
[16] K. A. Bush, C. D. Bailie, Y. Chen, A. R. Bowring, W. Wang, W. Ma, T. Leijtens, F. Moghadam, M. D. McGehee, *Adv. Mater.* **2016**, *28*, 3937.
[17] B. Chen, Y. Bai, Z. Yu, T. Li, X. Zheng, Q. Dong, L. Shen, M. Boccard, A. Gruverman, Z. Holman, J. Huang, *Adv. Energy Mater.* **2016**, 1601128.
[18] L. Kranz, A. Abate, T. Feurer, F. Fu, E. Avancini, J. Löckinger, P. Reinhard, S. M. Zakeeruddin, M. Grätzel, S. Buecheler, A. N. Tiwari, *J. Phys. Chem. Lett.* **2015**, *6*, 2676.
[19] F. Fu, T. Feurer, T. Jager, E. Avancini, B. Bissig, S. Yoon, S. Buecheler, A. N. Tiwari, *Nat. Commun.* **2015**, *6*, 8932.
[20] Y. Yang, Q. Chen, Y.-T. Hsieh, T.-B. Song, N. D. Marco, H. Zhou, Y. Yang, *ACS Nano* **2015**, *9*, 7714.
[21] J. P. Mailoa, C. D. Bailie, E. C. Johlin, E. T. Hoke, A. J. Akey, W. H. Nguyen, M. D. McGehee, T. Buonassisi, *Appl. Phys. Lett.* **2015**, *106*, 121105.
[22] T. Todorov, T. Gershon, O. Gunawan, Y. S. Lee, C. Sturdevant, L.-Y. Chang, S. Guha, *Adv. Energy Mater.* **2015**, *5*, 1500799.
[23] J. Werner, C.-H. Weng, A. Walter, L. Fesquet, J. P. Seif, S. De Wolf, B. Niesen, C. Ballif, *J. Phys. Chem. Lett.* **2016**, *7*, 161.
[24] J. Werner, L. Barraud, A. Walter, M. Bräuninger, F. Sahli, D. Sacchetto, N. Tétreault, B. Paviet-Salomon, S.-J. Moon, C. Allebé, M. Despeisse, S. Nicolay, S. De Wolf, B. Niesen, C. Ballif, *ACS Energy Lett.* **2016**, *1*, 474.
[25] S. Albrecht, M. Saliba, J. P. Correa Baena, F. Lang, L. Kegelmann, M. Mews, L. Steier, A. Abate, J. Rappich, L. Korte, R. Schlatmann, M. K. Nazeeruddin, A. Hagfeldt, M. Gratzel, B. Rech, *Energy Environ. Sci.* **2016**, *9*, 81.
[26] J. H. Heo, S. H. Im, *Adv. Mater.* **2016**, *28*, 5121.
[27] F. Jiang, T. Liu, B. Luo, J. Tong, F. Qin, S. Xiong, Z. Li, Y. Zhou, *J. Mater. Chem. A* **2016**, *4*, 1208.
[28] D. P. McMeekin, G. Sadoughi, W. Rehman, G. E. Eperon, M. Saliba, M. T. Hörantner, A. Haghighirad, N. Sakai, L. Korte, B. Rech, M. B. Johnston, L. M. Herz, H. J. Snaith, *Science* **2016**, *351*, 151.
[29] Z. Yang, A. Rajagopal, C.-C. Chueh, S. B. Jo, B. Liu, T. Zhao, A. K. Y. Jen, *Adv. Mater.* **2016**, *28*, 8990.
[30] M. Riede, C. Uhrich, J. Widmer, R. Timmreck, D. Wynands, G. Schwartz, W.-M. Gnehr, D. Hildebrandt, A. Weiss, J. Hwang, S. Sundarraj, P. Erk, M. Pfeiffer, K. Leo, *Adv. Funct. Mater.* **2011**, *21*, 3019.
[31] H. Sasabe, J. Kido, *J. Mater. Chem. C* **2013**, *1*, 1699.
[32] S. Reineke, M. Thomschke, B. Lüssem, K. Leo, *Rev. Mod. Phys.* **2013**, *85*, 1245.
[33] K. Walzer, B. Maennig, M. Pfeiffer, K. Leo, *Chem. Rev.* **2007**, *107*, 1233.
[34] M. Sessolo, C. Momblona, L. Gil-Escrig, H. J. Bolink, *MRS Bull.* **2015**, *40*, 660.
[35] L. K. Ono, M. R. Leyden, S. Wang, Y. Qi, *J. Mater. Chem. A* **2016**, *4*, 6693.
[36] T. J. Coutts, K. A. Emery, J. Scott Ward, *Prog. Photovolt: Res. Appl.* **2002**, *10*, 195.
[37] O. Malinkiewicz, A. Yella, Y. H. Lee, G. M. Espallargas, M. Graetzel, M. K. Nazeeruddin, H. J. Bolink, *Nat. Photonics* **2014**, *8*, 128.
[38] C. Momblona, L. Gil-Escrig, E. Bandiello, E. M. Hutter, M. Sessolo, K. Lederer, J. Blochwitz-Nimoth, H. J. Bolink, *Energy Environ. Sci.* **2016**, *9*, 3456.
[39] P.-W. Liang, C.-C. Chueh, S. T. Williams, A. K. Y. Jen, *Adv. Energy Mater.* **2015**, *5*, 1402321.
[40] L. Gil-Escrig, C. Momblona, M. Sessolo, H. J. Bolink, *J. Mater. Chem. A* **2016**, *4*, 3667.